Published in final edited form as:
J Opt Soc Am A Opt Image Sci Vis. 2007 May ; 24(5): 1431–1437.

Imaging polarimetry and retinal blood vessel quantification at the epiretinal membrane

Masahiro Miura
Department of Ophthalmology, Tokyo Medical University, 6-7-1 Nishi-Shinjuku, Shinjuku, Tokyo 1600023, Japan

Ann E. Elsner
School of Optometry, Indiana University, 800 East Atwater Avenue, Bloomington, Indiana 47405, USA

Michael C. Cheney
Atlantis Components, Inc., 25 First Street, Cambridge, Massachusetts 02141, USA

Masahiko Usui and **Takuya Iwasaki**
Department of Ophthalmology, Tokyo Medical University, 6-7-1 Nishi-Shinjuku, Shinjuku, Tokyo 1600023, Japan

Abstract

We evaluated a polarimetry method to enhance retinal blood vessels masked by the epiretinal membrane. Depolarized light images were computed by removing the polarization retaining light reaching the instrument and were compared with parallel polarized light images, average reflectance images, and the corresponding images at 514 nm. Contrasts were computed for retinal vessel profiles for arteries and veins. Contrasts were higher in the 514 nm images in normal eyes but higher in the depolarized light image in the eyes with epiretinal membranes. Depolarized light images were useful for examining the retinal vasculature in the presence of retinal disease.

1. INTRODUCTION

Epiretinal membranes (ERMs) are fibrocellular growths in the most superficial tissues of the retina,[1] commonly found in adults after the vitreous detaches from the retina. Contraction or shrinkage of ERMs causes varying degrees of visual disturbance,[1] and the retinal vessels may be stretched or compressed along with the neural tissue. The presence of strong specular reflections from the gliotic tissue in an ERM leads to the retinal vasculature being obscured.[2] These and similar membranous formations are not uncommon findings in retinal disease, such as proliferative diabetic retinopathy, and interfere with the detection of retinal vascular pattern by the eyecare specialist or in automatic detection for screening. Even in the presence of poor image quality for the retinal vessels and lesion components, ERMs are routinely removed surgically by a variety of techniques.[3] With the retinal vascular pattern often poorly delineated, there is limited knowledge concerning potential ischemia or prospective estimation of improvement in vision. Both surgical success and subsequent visual improvement are variable,[4] and improved diagnostic imaging may help overcome the reflection at ERMs and provide clear retinal vascular images.

Corresponding author M. Miura's e-mail address is m-miura@tokyo-med.ac.jp..

In a variety of diseases with a retinal vascular component, accurate and reproducible detection of retinal blood vessels improves computer-based automatic detection of retinal disease, and biometrics for individual identification using retinal vascular pattern technology.[5] Optimal imaging and analysis techniques are required to obtain the clear images of the retinal blood vessels in the abnormal retina, since the complex light-tissue interactions are inherent in retinal vascular images.[6]

The wavelength of illuminating light in retinal images has been emphasized as a factor influencing the contrast of retinal vessels.[7,8] In a study using a monochromatic fundus camera, the small retinal blood vessels had good contrast at wavelengths between 510 and 570 nm.[8] Monochromatic images over a wide range of wavelengths, including the short wavelengths found in red-free photography, are readily obtained using the scanning laser ophthalmoscope (SLO). Using an incident laser with a narrow spectral band in the short wavelength region, retinal vessels could be observed with high contrast. The illumination of only one point at a time prevents scattering over long distances from adjacent structures.[9] SLO images at short wavelengths can provide high-contrast images of the retinal vessels,[10] but the contrast with near-infrared illumination approaches images with short-wavelength illumination,[11] and is far better than in flood-illuminated fundus photography that lacks confocal apertures or adaptive optics. Short-to-medium-wavelength illumination that makes use of relatively high blood absorption with respect to melanin absorption, rather than merely lights that appear blue, can produce excellent images in the presence of clear media, e.g., 514, 532, 543, or 595 nm.[9,11,12]

Another important factor is light-tissue interaction at the retinal blood vessel.[6,13,14] Retinal vascular images are usually acquired using double-pass equipment. Returning light is a function of reflected, backscattered, and absorbed light from the fundus. Absorption by blood in a retinal vessel and backward multiple scattering from deeper layers are the main contributions to Beer's law, governing the potential contrast that can be obtained from retina vessels. The specular reflection at the retinal surface or retinal vessel wall can decrease the contrast of retinal vessels.[14] The most superficial layers of the retina and the vitreo–retinal interface provide a strong return of light relative to the deeper layers in a healthy eye, even with near-infrared illumination.[15] With the presence of membranous formation at the retinal surface, the superficial layers of the retina become even stronger reflectors and obstruct retinal vascular images.[2]

Recently, a polarimetry technique was developed to selectively emphasize the different components of light–tissue interactions at the retina, using an instrument that is highly confocal.[14,16-19] Using an incomplete polarimeter, multiply scattered light returning from deeper layers could be emphasized by computationally removing the polarization preserving portion of the light returning from an image series that varies in input polarization. We assume that light that does not modulate with polarization angle has become randomly polarized due to multiple scattering.[14,16-19] Using the depolarized light image, contrast of the retinal vessels is improved in two ways when compared with images in which the polarization content is not analyzed. First, the unwanted specular reflex at the center of each vessel is eliminated, and higher contrast of the retinal vessels compared with the neighboring retina is obtained because there is no bright stripe that can merge into the edge of the retinal vessel, particularly with small to medium vessels. Second, the bright reflection from the vitreo–retinal interface and nerve fiber layer is also removed, which otherwise adds a globally bright signal across the retina, including over the blood vessels.[14] In this study, we compared the effectiveness of visualizing the retinal vessels at ERMs with polarimetry images, as compared with SLO images at 514 nm. We hypothesize that 514 nm light images will provide high-contrast images in the presence of clear media for normal subjects, and that the depolarized light images will have similar or only slightly worse contrast. However, in the presence of ERM, we hypothesize that

the 514 nm images will no longer have the best contrast, and that the depolarized light images will provide better contrast.

2. METHODS

A. Subjects

We prospectively examined 24 eyes of 24 Japanese patients, 8 males and 16 females, 51–79 years (mean: age 65.0 years), with ERMs. A group of age-matched normal subjects: 24 eyes of 24 Japanese subjects, age 49–80 years (mean: age 65.1 years) were also examined. There was no significant difference in age between ERM patients and normal subjects (P=0.96, t test). Eyes with any prior intraocular surgery were excluded from the study. All eyes had sufficiently clear media for obtaining good quality polarimetry images and SLO images at 514 nm. Before testing, all subjects received a detailed explanation of the study procedure and signed consent forms approved by the Institutional Review Board of Tokyo Medical University.

B. Instrumentation and Polarization Computations

We used data from a commercially available ellipsometer, GDx-N (Laser Diagnostic Technologies, San Diego), an incomplete polarimeter that has a confocal aperture of roughly 30 μm, less than an order of magnitude larger than the illumination spot on the retina (Fig. 1). This instrument is a SLO that was originally developed for measuring the thickness of nerve fiber layers.[20] Linearly polarized light at 780 nm scans the retina in a raster pattern, 15° by 15° visual angle. To minimize unrelated corneal birefringence, the GDx-N uses a fixed compensator with a magnitude of 60 nm and a polarization axis of 15° nasally downward (single-pass retardance), which is uniform across the pupil plane. The returning light is separated into two beams by a rotating polarizing beam splitter: light of the same polarization as the illumination light, digitized at the parallel polarized detector, and light polarized at 90° to the illumination light, digitized at the crossed detector. There are 20 image pairs that vary systematically in illumination polarization angle, and each image in the series is saved as 256 × 256 pixels with 8 bits of gray scale. Acquisition time was less than 1 s for an image series.

The details of our computation for polarimetry images have been described in detail previously.[14,16-19] We developed a set of MATLAB routines (The Mathworks, Natick, Massachusetts) to compute depolarized light image, parallel polarized light image, and average reflectance image (Fig. 2). After correction for eye movement, we computed polarimetry images. The depolarized light image was computed as the minimum value of light returning to the crossed detector at each pixel for all input polarization angles. A parallel polarized light image was computed as the average intensity for the parallel polarized light minus the depolarized light contribution at each pixel. This value represents the average of amount of light, reaching the parallel detector that retains its original polarization, with the amplitude displayed in gray scale and independent of input polarization angle. An average reflectance image was computed as the grand mean of the light returning to both detectors for all input polarization states. In the average reflectance image, the light returns either to the crossed or uncrossed detector, with no light component systematically removed. Thus the average reflectance image, which combines all light returning from the 20 input polarization angles, is similar to that obtained with a typical confocal SLO with polarization insensitive detectors.

SLO images at 514 nm of 40° by 25° were digitized using the Rodenstock SLO (Rodenstock, Inc., München, Germany) with a confocal aperture of 800 μm with respect to the retina. Each image was manually aligned to the computed polarimetry images to have the same magnification as 256 × 256 pixels with 8 bits of gray scale.

C. Data Analysis

To calculate the contrasts of the retinal blood vessels, one retinal arteriole and one retinal venule were selected at 5° from the fovea of each eye. The first author selected those retinal vessel pairs large enough to provide sufficient samples for quantitative comparisons that could reach statistical significance. We used semiautomatic measurements of blood vessel intensity distribution (Fig. 3),[14,19] but for this study modified the algorithm to allow analysis of images with a broader variety of file formats. This algorithm is based on the idea that blood vessels tend to have features that are longitudinally homogeneous. An operator selected two points as the starting points, one on each side of a retinal vessel. The algorithm created 11 parallel lines along the line formed by the original two points, roughly perpendicular to the retinal vessel. Then the set of lines is rotated by ±20° in 2° increments to optimize the vessel intersection angles. The MAT-LAB algorithm did not resample the image during rotation, but rather placed each point in the sample for each of the 11 lines on the nearest pixel. For each of the 11 parallel dissector lines at given rotation angles, the minimum image intensity value is found, and its location over 11 bisector lines is recorded. The algorithm then calculated the standard deviation of this location over the 11 lines. The perpendicular bisector line was defined as the angle that minimizes the standard deviation of the locations of the minimum values in bisector lines. Then the average blood vessel profile was calculated (Fig. 3). The 11 bisector lines were averaged to reduce noise. Resampling of images occurred when figures were output for publication, which did not affect the computations.

To compare the retinal vessel profiles, we computed Michelson contrast of retinal vessels.

$$C=(L_{\max}-L_{\min})/(L_{\max}+L_{\min}), \quad (1)$$

where C is the Michelson contrast of retinal vessel. $L_{\max}$ is the average gray scale from the two most peripheral points on either side of the vessel profile, and $L_{\min}$ is the average gray scale at the darkest point. Intensities of the computed polarimetry images varied widely, and as expected the depolarized light images and birefringence images were too dark for subjective evaluation without further manipulation. For better visualization for selection of features for computations and publication, the distribution of intensities in each image was adjusted as follows: minimum to maximum intensities in the images were converted to a gray scale that ranged from 0 to 256 gray-scale units (Adobe Photoshop, San Jose, California). All statistical comparisons are performed on the original data. We used Michelson contrast as our measure, since it minimizes the influence of overall intensity, whether due to laser power differences among instruments or reflectivity of the ocular fundus for differing wavelengths. Michelson contrasts were compared for each polarimetry image and SLO image at 514 nm, for normal subjects and patients, and for arteries and veins, with analysis of variance (ANOVA) and paired *t* test.

3. RESULTS

In the normal retinas, clear retinal vascular images were obtained for each polarimetry image and SLO image at 514 nm (Figs. 4 and 5). The reflections at the center of the retinal vessels were significantly reduced in the depolarized light images. In other images, the reflections at the center of the vessels were clearly observed at the major retinal arteries. In all eyes with ERMs, retinal vessels were clearly visible in the depolarized light images (Figs. 6 and 7). More vessels were detectable, and these were uniformly dark in appearance. However, the retinal vessels had abnormal configurations, tortuous or stretched to the point of being straight. In other polarization image types shown, as well as the 514 nm images, the retinal vessels were considerably obscured by ERMs.

In normal eyes, the contrasts at retinal arteries and veins were significantly different according to image type (Fig. 8) ($P < 0.0001$ for both arteries and veins, ANOVA). The order, from highest contrast to lowest was: 514 nm > depolarized> average > parallel. In ERM eyes, again the contrasts at retinal arteries and veins were significantly different according to image type (Fig. 9) ($P < 0.0001$ for both arteries and veins, ANOVA). However, the order of contrasts at retinal arteries and retinal veins was different from that of normal subjects: depolarized > average > parallel > 514 nm. For normal subjects, the contrast in 514 nm images were significantly greater than in depolarized light images for retinal arteries and veins (P=0.032 and 0.001, respectively, paired t test). For patients with an ERM, the contrasts in depolarized light images were significantly greater than in the 514 nm light images for retinal arteries and veins ($P < 0.001$ for arteries and veins, paired t test).

4. DISCUSSION

In the current study, we evaluated polarization analysis as a noninvasive technique for the evaluation of retinal vascular changes visualized in image of ERMs. Polarization analysis can selectively emphasize different optical contributions from the retina. In the depolarized light images, the retinal vascular pattern in the presence of ERMs was readily visualized, indicating that detection of multiply scattered light is one way to improve retinal vascular imaging in the presence of ERMs.

The spectral properties of the illumination source have been discussed as important for retinal vascular images.[7,8] In the normal retina, retinal vessels were of high contrast with a SLO image with short-wavelength illumination. With the presence of an ERM, the same short wavelength yielded retinal vascular images with obstruction of the view of the vessels by membranous formation. This interference by membranous formation could be eliminated by using longer wavelength illumination, and contrast of retinal vessels could be improved. Among the images with near-infrared illumination, the depolarized light image is better than average reflectance images and parallel polarized light images. The depolarized light image has a major contribution from multiply scattered light[21,22] from deep retinal layers,[14,16-19] and the image of a dark retinal vessel on a lighter background depends upon on the Beer's law absorption of light that is passing through the blood as opposed to around the vessel.[14] An ERM is a strong reflector, and the specular reflex at the ERM forms an obstruction of clear retinal vascular images. The depolarized light image can eliminate the specular reflex at the retinal vessel, and also overcome the interference by the ERM. Consequently, the depolarized light image at long-wavelength illumination provides an improved imaging technique for visualizing retinal vessels in the same area as an ERM. Polarimetry images will allow more accurate measurement of absorption components of the light tissue interactions of the blood vessels at the ERM. This technique can help reduce the artifact or noise of the measurement of the optical properties at the retinal blood vessels, such as the reflection from the top of retinal vessels in oximetry.[6] Our method incorporates an incomplete polarimeter, which may not minimize the contribution of unwanted polarization-retaining light to the extent that full Mueller matrix polarimetry could,[22,23] has provided a related measurement of degree of polarization.[14,16] Assuming that half the depolarized light reaches the crossed detector, and the other half reaches the parallel detector, then a pointwise estimate of ratio of depolarized light to the total is one image type of 18 that we regularly compute. However, while subtracting from a unity image provides an image that is an estimate of degree of polarization, this type of computation confounds the two light components that we are trying to separate: (1) light retroreflected from deeper structures and passes through the blood vessels, and (2) light that returns mostly from more superficial structures. The GDx-N is a highly confocal instrument with a fixed corneal compensator,[24] which for a given image in the series provides nearly uniform polarization conditions to each point scanned on the retina. However, the GDx-N does not allow for variations of the confocal aperture size, which may be too small to optimize the

contribution of scattered light in the depolarized light image.[25] Polarization methodologies that incorporate novel instrumentation or image analysis to emphasize specific data features or types of tissues, such as our method to enhance blood vessels by removing the unwanted specular reflections regardless of vessel orientation, polarization difference imaging, and new methods with principal components analysis.[26-29]

5. SUMMARY AND CONCLUSION

In this paper, we studied a polarimetry method to examine retinal blood vessels in a retinal area containing an epiretinal membrane. In normal eyes, contrasts of retinal arteries and veins were higher in the 514 nm image. With a presence of membranous formation on the retinal surface, retinal vascular images were interfered in 514 nm images, and clear retinal vascular images were obtained with a depolarized light image. This result suggests polarimetry methods are an effective tool for visualizing retinal vessels in eyes with retinal disease.

References

1. Gass, JDM. Stereoscopic Atlas of Macular Disease. 3. Mosby; 1987.
2. Ogura Y, Honda Y. Evaluation of idiopathic epiretinal membranes by a scanning laser ophthalmoscope. Br J Ophthamol 1993;77:534–535.
3. Rizzo S, Genovesi-Ebert F, Murri S, Belting C, Vento A, Cresti F, Manca ML. 25-gauge, sutureless vitrectomy and standard 20-gauge pars plana vitrectomy in idiopathic epiretinal membrane surgery: a comparative pilot study. Graefe's Arch Clin Exp Ophthalmol 2006;244:472–479.
4. Scott IU, Smiddy WE, Merikansky A, Feuer W. Vitreoretinal surgery outcomes. Impact on bilateral visual function. Ophthalmology 1997;104:1041–1048. [PubMed: 9186447]
5. Patton N, Aslam TM, MacGillivray T, Deary IJ, Dhillon B, Eikelboom RH, Yogesan K, Constable IJ. Retinal image analysis: concepts, applications and potential. Prog Retin Eye Res 2006;25:99–127. [PubMed: 16154379]
6. Hammer M, Leistritz S, Leistritz L, Schweitzer D. Light paths in retinal vessel oxymetry. IEEE Trans Biomed Eng 2001;48:592–598. [PubMed: 11341533]
7. Park R, Twietmeyer K, Chipman R, Beaudry N, Salyer D. Wavelength dependence of the apparent diameter of retinal blood vessels. Appl Opt 2005;44:1831–1837. [PubMed: 15813519]
8. Delori FC, Gragoudas ES, Francisco R, Pruett RC. Monochromatic ophthalmoscopy and fundus photography. The normal fundus. Arch Ophthalmol (Chicago) 1977;95:861–868. [PubMed: 860947]
9. Elsner AE, Burns SA, Hughes GW, Webb RW. Reflectometry with a scanning laser ophthalmoscope. Appl Opt 1992;31:3697–3710.
10. Kirkpatrick JN, Manivannan A, Gupta AK, Hipwell J, Forrester JV, Sharp PF. Fundus imaging in patients with cataract: role for a variable wavelength scanning laser ophthalmoscope. Br J Ophthamol 1995;79:892–899.
11. Elsner, AE.; Burns, SA.; Delori, FC.; Webb, RH. Quantitative reflectometry with the SLO. In: Nasemann, JE.; Burk, ROW., editors. Laser Scanning Ophthalmoscopy and Tomography. Quintessenz-Verlag; 1990. p. 109-121.
12. Elsner AE, Burns S, Weiter J, Delori F. Infrared imaging of subretinal structures in the human ocular fundus. Vision Res 1996;36:191–205. [PubMed: 8746253]
13. Bartsch DU, Freeman WR. Laser-tissue interaction and artifacts in confocal scanning laser ophthalmoscopy and tomography. Neurosci Biobehav Rev 1993;17:459–467. [PubMed: 8309654]
14. Weber A, Cheney MC, Smithwick QYJ, Elsner AE. Polarimetric imaging and blood vessel quantification. Opt Express 2004;12:5178–5190.
15. Miura M, Elsner AE. Three-dimensional imaging in age-related macular degeneration. Opt Express 2001;9:436–443.
16. Burns SA, Elsner AE, Mellem-Kairala MB, Simmons RB. Improved contrast of subretinal structures using polarization analysis. Invest Ophthalmol Visual Sci 2003;44:4061–4068. [PubMed: 12939329]

17. Miura M, Elsner AE, Weber A, Cheney MC, Osako M, Usui M, Iwasaki T. Imaging polarimetry in central serous chorioretinopathy. Am J Ophthalmol 2005;140:1014–1019. [PubMed: 16376644]
18. Mellem-Kairala MB, Elsner AE, Weber A, Simmons RB, Burns SA. Improved contrast of peripapillary hyperpigmentation using polarization analysis. Invest Ophthalmol Visual Sci 2005;46:1099–1106. [PubMed: 15728571]
19. Elsner AE, Miura M, Stewart JB, Kairala MB, Burns SA. Novel algorithms for polarization imaging resulting in improved quantification of retinal blood vessels. Stud Health Technol Inform 2003;94:59–61. [PubMed: 15455864]
20. Dreher AW, Reiter K, Weinreb RN. Spatially resolved birefringence of the retinal nerve fiber layer assessed with a retinal laser ellipsometry. Appl Opt 1992;31:3730–3735.
21. Demos SG, Alfano RR. Optical polarization imaging. Appl Opt 1997;36:150–155. [PubMed: 18250656]
22. Bueno JM. Polarimetry in the human eye using an imaging linear polariscope. J Opt A, Pure Appl Opt 2002;4:553–561.
23. Chipman, RA. Polarimetry. In: Bass, M., editor. Handbook of Optics. 2. 2. McGraw-Hill; 1995. p. 1-28.
24. Zhou Q, Weinreb RN. Individualized compensation of anterior segment birefringence during scanning laser polarimetry. Invest Ophthalmol Visual Sci 2002;43:2221–2228. [PubMed: 12091420]
25. Elsner AE, Moraes L, Beausencourt E, Remky A, Weiter J, Walker J, Wing G, Burns SA, Raskauskas P, Kelley L. Scanning laser reflectometry of retinal and subretinal tissues. Opt Express 2000;6:243–250.
26. Dogariu M, Asakura T. Polarization-dependent backscattering patterns from weakly scattering media. J Opt (Paris) 1993;24:271–278.
27. Tyo JS, Rowe MP, Pugh EN, Engheta N. Target detection in optically scattering media by polarization-difference imaging. Appl Opt 1996;35:1855–1870.
28. LeRoyBrehonnet F, LeJeune B, Gerligand PY, Cariou J, Lotrian J. Analysis of depolarizing optical targets by Mueller matrix formalism. Pure Appl Opt 1997;6:385–404.
29. Yemelyanov KM, Lin SS, Pugh EN Jr, Engheta N. Adaptive algorithms for two-channel polarization sensing under various polarization statistics with nonuniform distributions. Appl Opt 2006;45:5504–5520. [PubMed: 16855649]

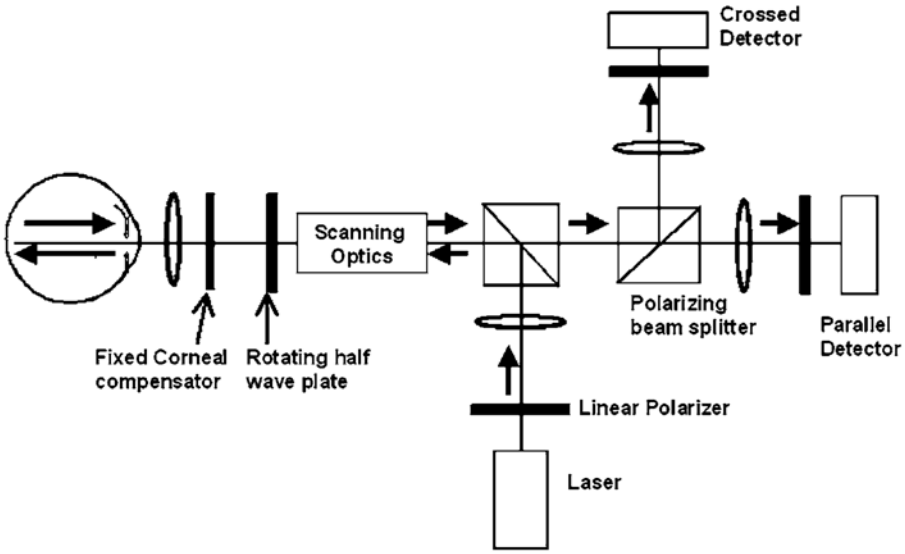

Fig. 1.
Schematic of GDx-N.

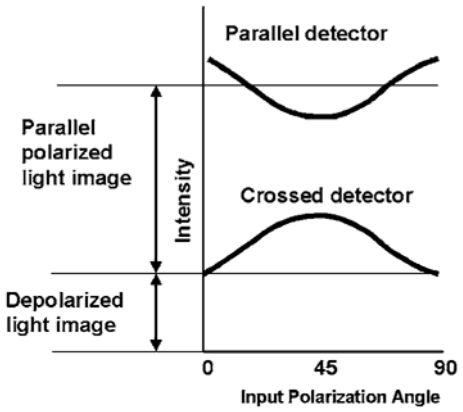

Fig. 2.
Schematic of the polarimetry algorithm that is used to compute different polarization content. Gray scale for one pixel is calculated for each of 20 polarization angles.

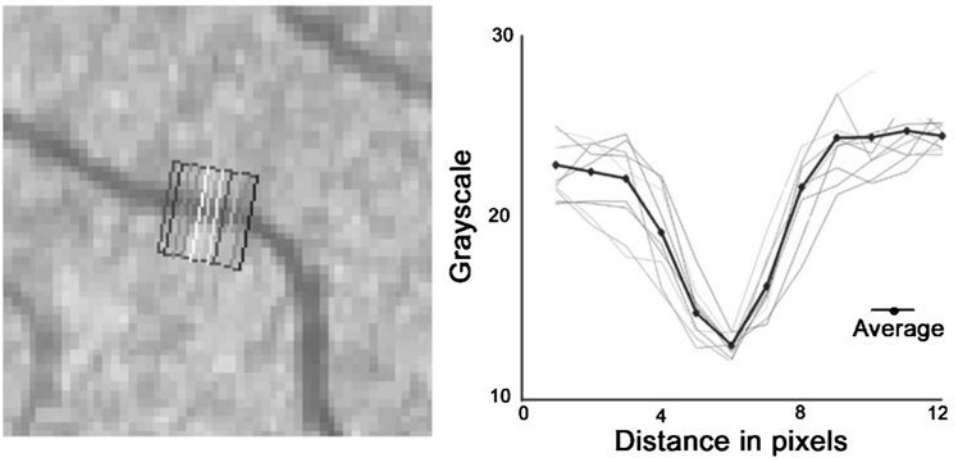

Fig. 3.

Vessel profiles across one artery in the depolarized light image of a normal subject. (Left) Eleven bisector lines were selected by a computer algorithm that finds adjacent parallel lines that are perpendicular to the vessel defined by selecting pixels on either side of the vessel. (Right) An average profile was calculated from the grayscale profile of 11 bisector lines.

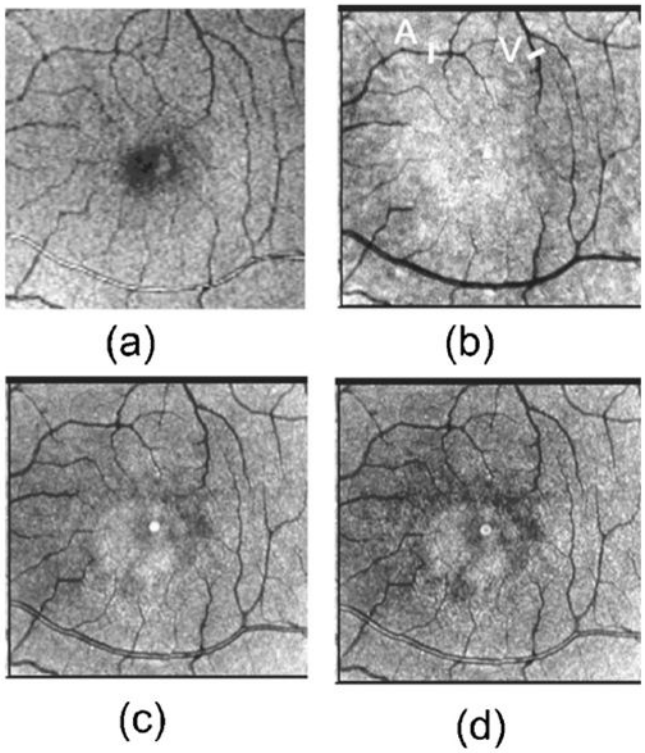

Fig. 4.

Retinal images of 66 year old Japanese man with a normal retina. (a) SLO image at 514 nm, (b) depolarized light images, (c) average reflectance image, (d) parallel polarized light image. SLO image at 514 nm, average reflectance image, and parallel polarized light image demonstrating the reflection at the center of the major retinal artery. This reflection was significantly reduced in the depolarized light images. Bar indicates the sample region for average vessel profiles of 11 bisector lines of retinal artery (A) and retinal vein (V). Bright spot in the center of each polarimetry image is an artifact due to internal reflections in the GDx-N.

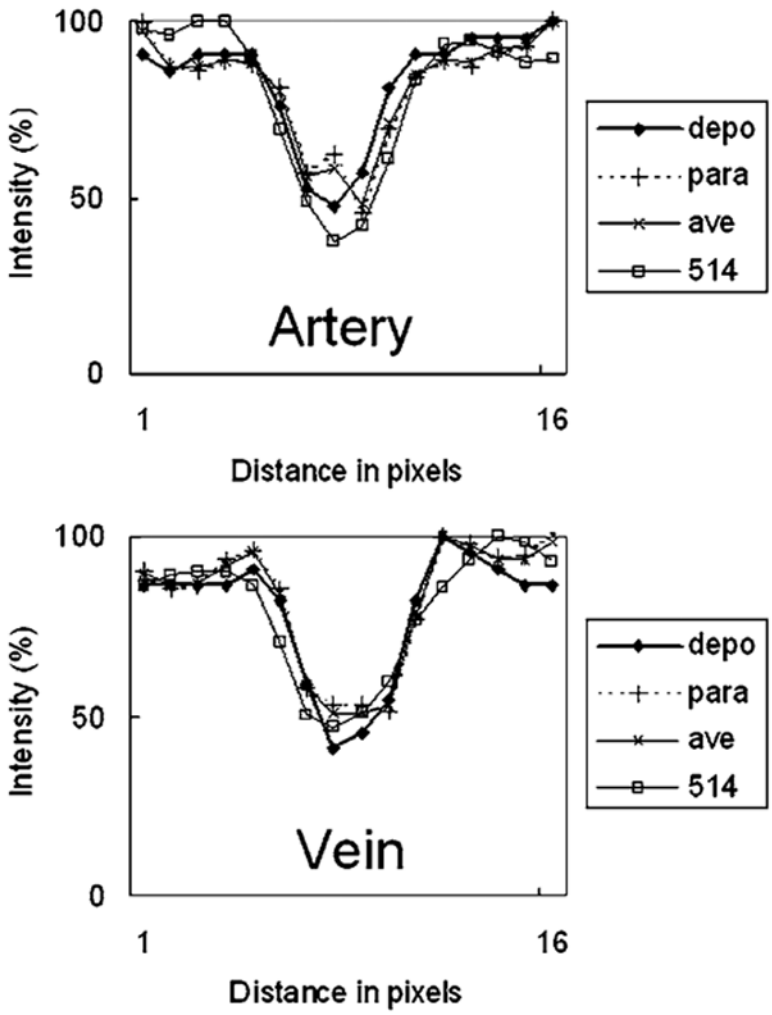

Fig. 5.

Computed data for blood vessel profiles of a retinal artery and a retinal vein, in Fig. 3. Each profile was plotted as a percentage of maximum grayscale unit in each profile, as a function of location in profile.

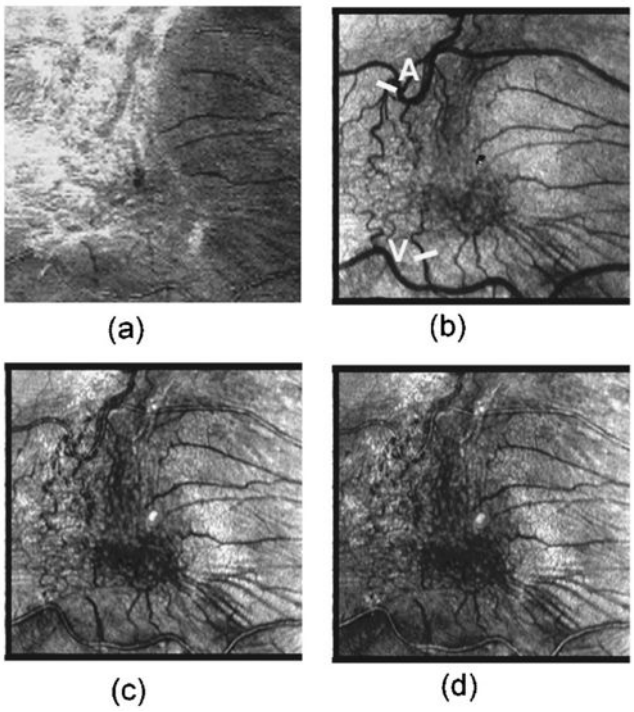

Fig. 6.

Retinal images of 70 year old Japanese man with an ERM. (a) SLO image at 514 nm, (b) depolarized light images, (c) average reflectance image, (d) parallel polarized light image. ERM could be clearly visualized as the highly reflected area in the SLO image at 514 nm. In the depolarized light image, the retinal vessels could be clearly visualized in the area of the ERM. In the average reflectance image and parallel polarized light image, the retinal vessels were somewhat obscured by the ERM. Bar indicates the sample region for average vessel profiles of 11 bisector lines of retinal artery (A) and retinal vein (V). Bright spot in the center of each polarimetry image is an artifact due to internal reflections in the GDx-N.

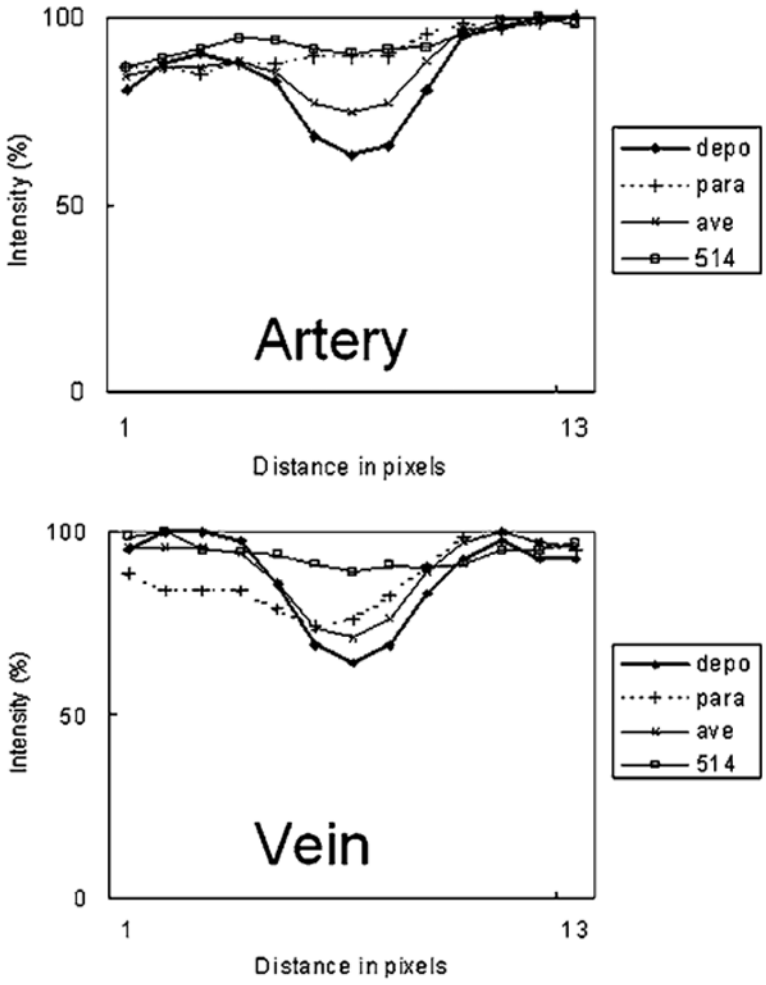

Fig. 7.

Computed data for blood vessel profiles of a retinal artery and a retinal vein, in Fig. 5. Each profile was plotted as a percentage of maximum grayscale unit in each profile, as a function of location in profile.

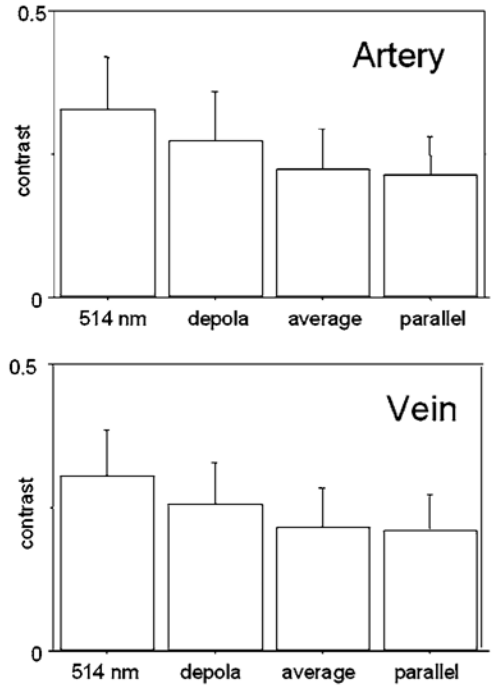

Fig. 8.

Michelson contrast of retinal arteries and veins in normal retinas. Contrast is greatest in SLO images at 514 nm. Error bars indicate standard deviation of Michelson contrast.

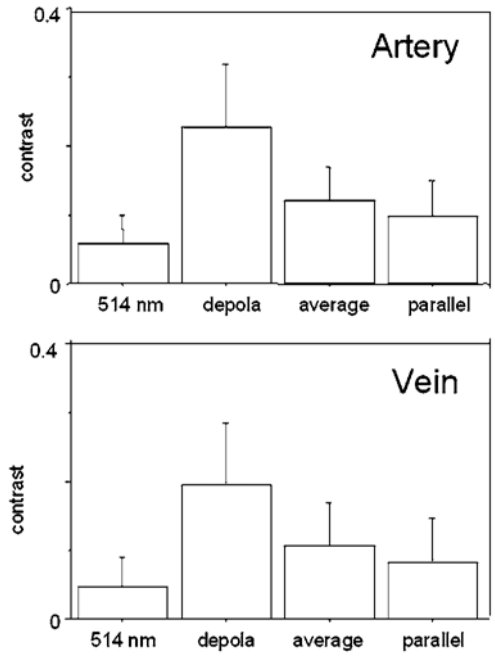

Fig. 9.

Michelson contrast of retinal arteries and veins in the eyes with ERMs. Contrast is greatest in the depolarized light image. Error bars indicate standard deviation of Michelson contrast.